CHAPTER 20

Dust storm characteristics over Indo-Gangetic basin through satellite remote sensing

Prashant Kumar Chauhan[a], Akhilesh Kumar[a,b], Vineet Pratap[a], Shivam Kumar Chaubey[a], Abhay Kumar Singh[a,c]

[a]Atmospheric Research Laboratory, Department of Physics, Institute of Science, Banaras Hindu University, Varanasi, Uttar Pradesh, India
[b]Kashi Naresh Government Post Graduate College Gyanpur, Bhadohi, India
[c]DST - Mahamana Centre of Excellence in Climate Change Research, Banaras Hindu University, Varanasi, India

20.1 Introduction

A dust storm is a meteorological phenomenon that happens when the intense wind blows loose sand and debris from a dry surface, which is most common in arid and desert areas [1]. During the premonsoon season, Indo-Gangetic basin (IGB) frequently experiences dust storms originated from mid-arid regions and Thar Desert [2,3]. Dust storms are mainly associated with a large uncertainty because of the different source regions, transportation, and complex atmospheric conditions and also the global climate models suggest the higher value of total global dust emission which is approximately 500–6000 Tg/year [4]. In aerosol loading, Dust is one of the most important constituents of which contributes nearly 30% of global aerosol optical thickness and 75% global aerosol mass load [5]. The dust particles mixed with fine mode anthropogenic aerosols are called brown carbon that increases the concentration of aerosol particles and can affect the biosphere, cryosphere, and eco-system of Earth [6,7]. They are also referred to the fraction of organics that shows light absorption characteristics from the near UV to the visible region. The air quality, atmospheric chemistry, vegetation, public health, and welfare are also affected by these dust particles [8].

Most of the dust storms originate from the desert and semidesert parts of the world and have various impacts on the Earth system and human society [9]. These dust hazards affect the environment, society, and livelihoods [9,10]. More than 100 people's deaths were reported because of very strong lightning and wind associated with an intense dust storm in northwestern India, in May 2018 (https://www.wunderground.com/cat6/fierce-thunderstorm-related-winds-kill-more-100/India). The main reasons for the deaths were many walls and roofs of the houses were collapsing and trees were falling onto the buildings due to the strong dust hazards. There were water shortages and power cuts because thousands of the electricity poles were blown [11]. Later in the same

Atmospheric Remote Sensing
DOI: https://doi.org/10.1016/B978-0-323-99262-6.00007-9

month, thousands of people were killed and millions of people were affected by a series of dust storms that covered a much wider area of central and southwest Asia, which affected the regions of northwestern states of India, northwestern parts of Pakistan, eastern regions of Iran, and some parts of Uzbekistan and Turkmenistan [12].

For the first time, an overview of dust storms was presented by Middleton [13]. Dust particles can perturb the Earth's radiation budget, which usually changes the temperature of the Earth's surface and lead to influence the exchange processes between the Earth's surface, atmosphere, and atmospheric dynamics. Because of their broad spatial distributions and large optical depths, it is very important to measure the accurate estimation of the radiative impact of dust storms [14]. Dust storms are transported over large distance from one place to another place and vertically up to 6–8 km which usually depends on the intensity of wind [15]. The IGB, one of the world's biggest basin, which frequently experiences dust storms during the premonsoon season (April–June) and carries a large number of dust particles, resulting in the enhancement of aerosol optical depth and reducing the solar radiation by nearly 50–100 W/m^2 at the surface [16,17]. Dust is transported from the Arabian Peninsula to the surrounding oceans and subsequently toward the Thar and IGP [2,18–20]. Depending upon meteorological conditions, wind velocity, wind direction, air temperature, boundary layer height, etc., the western parts of India were first affected by these dust storms and then it entered the IGB and was transported toward the eastern parts of India. Remote sensing data has been used to measure severe dust loading across the IGB during the premonsoon season [21].

Dust storm causes serious health risk to human health [22]. The size of the dust particles is the key factor in determining the possible risk to human health. The larger particle of size larger than 10 μm are not breathable, may affect the external organs like eye and skin infection, ocular infection, and conjunctivitis [22]. Smaller particles of size less than 10 μm are inhalable, may cause respiratory disorders like Tracheitis, Asthma, and Allergic rhinitis, etc., because these particles may enter and get trapped in the nose and upper respiratory tract [23]. However, the finer particles can enter the lower respiratory tract and in the bloodstream and may affect the internal organs, causing cardiovascular disorder [24]. There was a global model assessment in 2004, gave an idea of estimation that dust particles cause premature deaths of about 400,000 by cardiopulmonary disease in the 30 and older years age population [25,26].

To study the dust storm characteristics, remote sensing techniques are well accepted. Remote sensing techniques are widely used for the detailed study of dust storm, their detection, transportation, and their path mapping [27]. When we study the dust storm by only use of satellite remote sensing technique, we observe that there is large uncertainty in measuring the accurate information of the dust storm; because there are different types of limitations of satellite remote sensing like cloud contamination, spatial distribution, and data retrievals algorithm, etc. Therefore to reduce these uncertainties and inaccuracy to dust storms, different researchers have studied dust storms by combined

Fig. 20.1 ***View of a dust storm on June 9, 2018 at Uttar Pradesh.*** (https://www.deccanherald.com/national/26-killed-dust-storms-lightning-674149.html)

use of satellite remote sensing, ground-based measurements of properties of dust particles, and modeled data over IGB [2,16,17]. Because dust particles are combined with anthropogenic aerosol particles, which collectively alter the Earth's atmosphere's radiative forcing, therefore it is highly needed to study the dust particles' characteristics over IGB [6,28,29]. For this fact, Prasad and Singh [30] studied long-term (2001–2005) dust storm characteristics over IGB using satellite and ground data. Some other researchers focused on some selected dust storms and studied the different dust characteristics like its path mapping and radiative forcing during these events over the Gangetic–Himalayan region [31], the Western Ghats [32], Delhi [17], Patiala [28,33], Kanpur [16,34]. During the premonsoon season, an enhancement in columnar water vapor is reported which may also increase radiative forcing which leads to net atmospheric warming [16,28]. It is also reported that during the dust events, there was an elevation in dust loading up to 4 km over the IGB [35]. The view of a dust storm that occurred on June 9, 2018 in Uttar Pradesh has been shown in Fig. 20.1 (https://www.deccanherald.com/national/26-killed-dust-storms-lightning-674149.html).

20.2 Data and methodology

20.2.1 AErosol RObotic NETwork (AERONET)

CIMEL Sun/Sky radiometer measurements data are used to find the characteristics of dust particles. In IGP, it is deployed at several locations under the AERONET program of NASA, USA. Kanpur is one of them. This instrument measures direct Sunlight at

eight different wavelengths within the range of 0.34–1.02 μm (0.34, 0.38, 0.44, 0.50, 0.67, 0.87, 0.94, and 1.02 μm). At these wavelengths, AOD and columnar water vapor (only at 0.94 μm) are obtained [36]. At four wavelengths (0.33, 0.67, 0.87, and 1.02 μm), it also provides diffuse sky radiance. With the help of this, we can obtain retrieve aerosol columnar volume size distribution (AVSD), phase function, refractive indices of aerosols, single scattering albedo (SSA), and asymmetry parameters (AP) by the inversion method [36,37]. Three different versions (1, 2, and 3) with three different categories, namely, (1) cloud contaminated (level 1.0), (2) cloud screened (level 1.5), and (3) quality assured (level 2.0) exist, respectively, at which data are online available [38]. Under the cloud-free condition, uncertainty in AOD calculation is less than ± 0.02 for shorter wavelengths and less than ±0.01 for higher wavelengths ($\lambda > 0.44$ μm); while uncertainties up to 10% occur in columnar water vapor [39,40]. For the particles of radius (R) in the range of 0.1–7 μm, the errors are insignificant. As the optical depth decreases, the tendency for errors in the retrieval of refractive index (RI) and SSA tends to increase more than in the volume size distribution [39].

20.2.2 Moderate-resolution imaging spectroradiometer (MODIS)

The moderate resolution imaging spectroradiometer (MODIS) has been installed for monitoring ocean, land, and atmosphere observations. This instrument is attached to the Terra and Aqua satellites, which were activated in December 1999 and May 2002, respectively [41]. MODIS instrument gives daily global data of dust characteristics like Radiance at 36 spectral bands in visible to thermal infrared of wavelength ranging from 0.41 to 14.38 μm [33]. Aerosol characteristics are retrieved within the channels at 0.41 μm to 2.1 μm while in the near-infrared range, information about water vapor is gathered through five channels [42]. Spatial elements are produced by aligning the detectors from the different bands, each containing 81 data channels. The MODIS provides various types of information (having spatial resolution 1 km) such as geodetic latitude and longitude, satellite zenith angle, satellite azimuth height above the earth ellipsoid, range to the satellite, solar azimuth, and solar zenith angle. MODIS scans the entire surface of the earth every 1 to 2 days. Terra and Aqua satellites cross over the Indian region at 10:30 a.m. and 01:30 p.m. IST [43]. MODIS data is accessible at the NASA Giovanni website (https://giovanni.gsfc.nasa.gov/giovanni/) without any cost. It is often used for scanning the earth's atmosphere [44]. Aerosol product by MODIS global level 3 at 1° spatial resolution is derived from level 2 MODIS product having 10 km resolution [42]. Characteristics of aerosol, water vapor, and parameters of ozone can be obtained from MODIS level 3 product in a single HDF file which is important to observe the interaction among aerosol, hydrological cycle, and energy budget [42]. Kumar et al. [16] examined that there was diverse loading of aerosol during dust events over IGB especially from west to east (22.5–32^0 N & 68–88^0 E) **(**Fig. 20.2A). Thick dust plumes are observed by MODIS over the Thar Desert. Initially, these plumes are a shift to the

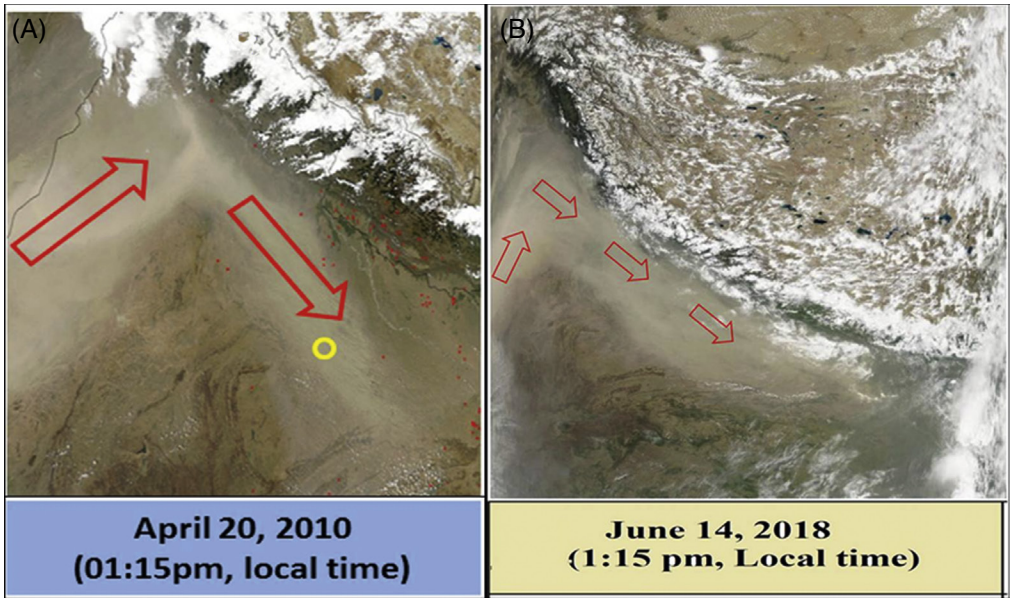

Fig. 20.2 MODIS TERRA true color images showing dust-storm events over IGB (A) on April 20, 2010 [16] and (B) on June 14, 2018 [43]. The dust appears in pale beige color, while clouds are appeared in white color and red arrows show the pathways of the dust plumes and yellow circle represents the location of Kanpur. (Source: http://rapidfire.sci.gsfc.nasa.gov).

northeast and then southeast (Fig. 20.2B). The plenty of dust that was propagating toward the northeast is deposited over the Himalayan foothills through which radiative balance is affected over this region [45].

20.2.3 Cloud-aerosol LIDAR and infrared pathfinder satellite observation (CALIPSO)

The Cloud-Aerosol LIDAR and Infrared Pathfinder Satellite Observations (CALIPSO) is a satellite developed by the National Aeronautics Space Administration (NASA) that measures the vertical profile of dust particles. It monitors atmospheric dust, its transport, and its vertical extent [46]. To study the vertical distribution, optical and physical characteristics of dust particles and clouds at 532 nm and 1064 nm, CALIPSO was launched on April 28, 2006 that discriminates between water and ice cloud and identifies the non-spherical dust particles [47]. Level 1 data of CALIPSO contains LIDAR calibrated profile while level 2 contains cloud layer products. Cloud-Aerosol LIDAR with Orthogonal Polarization (CALIOP) is the main instrument mounted on the CALIPSO. CALIOP measures the ice-water phase with the help of LIDAR backscatter signal depolarization or particle depolarization ratio (PDR) and color ratio (CR) under the sky conditions whereas it cannot observe below thick clouds. As CR measures the size

of a particle, it can be calculated by comparing its backscatter coefficient at 1064 nm to that at 532 nm. With the help of PDR, the shape of the particle is measured by dividing the parallel backscatter coefficient by the perpendicular scatter coefficient at 532 nanometers [16]. The presence of large and nonspherical particles is confirmed by the higher values of CR (>0.6) and PDR (>0.2) while smaller values are the indication of small and spherical particles [48,49]. CALIPSO's orbit has a period of 16 days that provides subsatellite paths spaced longitudinally by 172 km at the equator. Spatial coverage by CALIPSO is less compared to MODIS as its observations are restricted to the subsatellite path [43]. CALIOP observations of total attenuated backscatter at 532 nm confirm that there is a higher concentration of dust particles over IGB [43].

20.2.4 Hybrid Single-Particle Lagrangian Integrated Trajectory (HYSPLIT)

The National Oceanic and Atmospheric Administration Air Resources Laboratory's Hybrid Single-Particle Lagrangian Integrated Trajectory Model (HYSPLIT) is a model that analyses the trajectories of an air parcel. To describe atmospheric transport, pollutant deposition, and dispersion, HYSPLIT plays an important role [50]. This model includes the Lagrangian approach in which a moving reference frame is used for the diffusion and advection as the air parcel shift its position and Eulerian methodology in which a fixed three-dimensional grid is used that measures the concentration of pollutant air [51]. HYSPLIT is used for measuring the five days back trajectories of air masses at three different heights of 1000, 1500, and 2000 m above mean sea level in most of the studies [52]. It can be easily calculated at the website http://ready.arl.noaa.gov/HYSPLIT.php. Kumar et al. [16] observed that Arabian Peninsula is the source of air masses at lower altitudes (1000 m), while the Middle East region is the source of air masses at high altitudes (1500 m, 2000 m). Tiwari et al. [43] showed that the Thar Desert is the origin of a higher concentration of dust particles over IGB on June 14, 2018.

20.3 Characteristics of dust particles

20.3.1 Physical and optical characteristics

20.3.1.1 Aerosol optical depth (AOD) and angstrom exponent (AE)

There are two very important parameters AOD and AE to know the characteristics of dust aerosol particles. AOD tells about the attenuation of light due to aerosol particles. Its value is equal to the negative logarithm of the radiation (scattered or absorbed) by the aerosol particles on a vertical path from the surface to the top of the atmosphere. AE gives information about the size of aerosol particles [53]. These parameters can be calculated easily by Eq. (20.1):

$$\tau_a(\lambda) = \beta \cdot \lambda^{-\alpha} \tag{20.1}$$

where τ_a is AOD for the wavelength λ, λ is the wavelength in micrometer, β is the turbidity coefficient, equals to columnar AOD at λ = 1 μm and α is angstrom exponent

Table 20.1 Aerosol characteristics and radiative forcing in previous studies over Gangetic–Himalayan region during the premonsoon season.

Study location	Dust storm event	AOD	AE	SSA	AVSD	SRF	TOA RF	References
Kanpur	08/05/2001	1.14	0.29	0.91	1.0441			[2]
	09/05/2001	1.28	0.16	0.94	1.086			
	19/05/2002	0.94	–	0.99	1.083			
	20/05/2002	1.81	0.0012	0.97	2.253			
	27/05/2002	1.40	0.04	0.98	1.583			
	09/04/2005	1.251	-0.007	0.963	0.666			
	08/05/2005	1.263	0.137	0.949	0.508			[42]
	03/06/2005	0.853	0.258	0.925	0.397	-87.5	-26	
	10/06/2005	1.446	0.105	0.918	0.993			
	11/06/2005	1.625	0.053	0.961	1.171			
Delhi	08/04/2005	2.99	0.087	–	–	–	–	[65]
Nainital	13/06/2006	0.63	0.04	0.79		-45.0	-30	[31]
Kanpur	20/04/2010	1.38	-0.049	0.919	–	-93.27	-18.16	[16]
	28/05/2010	1.192	0.071	0.904	–	-101.6	-40.95	
	03/06/2010	1.31	0.023	0.969	–	-66.71	-29.58	
Delhi	21/03/2012	0.74	-0.02	–	–	-86.0	–	[66]
Kanpur	17/05/2018	1.11	0.366	0.89	0.694	-160.45	-36.06	[43]
	14/06/2018	2.52	0.067	0.93	1.076	-141.45	-56.51	
Patiala	21/04/2010	1.13	0.31	0.925	–	-75.9	-16.4	[33]
	28/05/2010	1.52	0.14	0.924	–	-102.6	-22.6	
	20/03/2012	1.55	0.35	0.88	–	-96.71	-19.66	[28]

(AE). The more the value of AOD, the higher is the concentration of aerosol particles within a column. The AE is a good indicator of the aerosol particle size distribution and fraction $r < 1$ μm tells about the accumulation mode while $r > 1$ μm tells about the coarse-mode particles quantitatively [54]. To study the different characteristics of dust particles during the major dust storm events, several works have been reported [2,42]. After analyzing the dust events of May and June 2018 over IGB, it was found that the monthly average of AOD in May and June was 0.89 ± 0.19 and 1.05 ± 0.43, respectively, whereas that of AE was 0.71 ± 0.21 and 0.60 ± 0.35, respectively. But during the dust event on May 17, 2018 AOD value became 1.1 which was enhanced by nearly 25% of the monthly mean value and the value of AE got decreased by nearly 50% which clearly showed the enhancement, of course-mode particles. While during the dust event on June 14, 2018, the AOD value increased by 2.4 times the monthly mean value and the value of AE decreased up to nearly zero value (Table 20.1) which tells about the abundance of dust particles into the atmosphere. During the dust storm occurred in 2010 also shows high value of AOD with lower value of AE along with their sources which is shown in Fig. 20.3A and B [16]. Similar studies like a sudden decrease in AE and increase in AOD during dust storm days were reported [2,16].

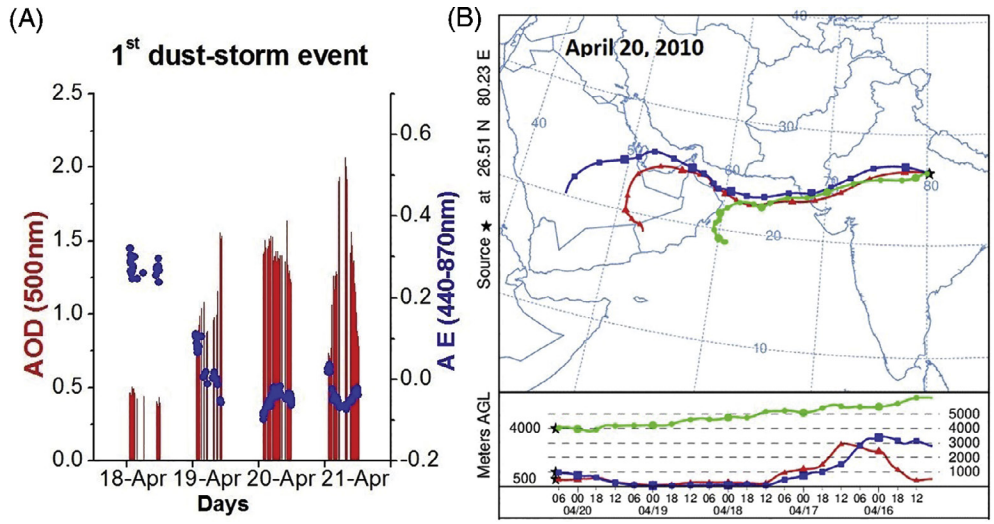

Fig. 20.3 (A) Daily (all point) variation of AOD (500 nm) and Ångström exponent (440–870 nm) at Kanpur AERONET site during the dust-storm events [16], (B) 5-days air mass back trajectory using HYSPLIT model over Kanpur station at three different altitudes.

20.3.1.2 Aerosol volume size distribution (AVSD)

The main symptom that slightly differentiates the optical properties of the dust aerosol from the anthropogenic and biomass burning aerosol is the abundance of coarse particles during the dust storm. Dust aerosols have a stronger absorption of solar and infrared wavelengths compared to aerosols that are influenced (directly or indirectly) by humans, e.g., sulfate.

The aerosol size distribution depends on emission sources, composition, transport patterns, and removal mechanisms. AVSD is a very important parameter that clearly shows a significant difference between dusty and premonsoon days. In Fig. 20.4, we can easily observe the variation of AVSD (dV/dlnr) with respect to the particles' radius

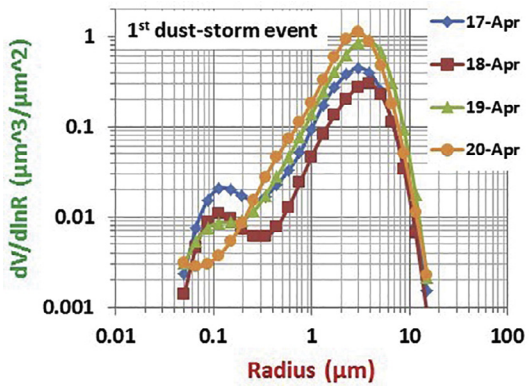

Fig. 20.4 Aerosol volume size distribution for 22 size bins between 0.05 and 15 µm at Kanpur AERONET station during the dust-storm events in premonsoon season [16].

from the fine to coarse mode particles (0.05 to 15 μm). The sun/sky radiometer data according to the approach of Dubovik and King [37] was used for the dust events in Kanpur on April 20, 2010, and are shown in Fig. 20.4 [16]. Significant increase in the concentration of coarse mode particle (as peak of AVSD shifted toward the coarse mode particles) in relation to the anthropogenic particles of fine mode during the dusty days was seen which can also be verified from the very small or even negative value of AE during the dusty days [3,31]. Previous studies had also reported a nearly similar volume size distribution for aerosol particles at the Kanpur station [2], in Karachi [55], and also in Delhi [17] during large dust storms in the premonsoon season.

20.3.1.3 Single scattering albedo (SSA)

One of the foremost vital properties of the dust aerosol properties is SSA which can give the data of approximate decrease in solar as well as terrestrial radiation in contaminated environments. It gives the point of interest data about the absorbing as well as scattering nature of the dust aerosol particles which is one of the key parameters for the calculation of the atmospheric radiative forcing (ARF). SSA has direct relation with ARF in the sense of reflectivity. High surface albedo corresponds to positive radiative forcing while low surface albedo corresponds to negative radiative forcing [56]. The effective method used to calculate SSA is by the scattering optical thickness gotten from the phase function of the normalized dust aerosol particles utilizing diffuse radiance which is measured at diverse angles and has a value ranging from zero to one, where one shows the value for completely scattering types of dust aerosol particles (e.g., sulfate) and zero for completely absorbing types of dust aerosol particles and exceedingly depends on size and composition of the dust aerosol particles [57]. Previously there were several studies done related to the SSA during the dust storm events and it was found that SSA shows an increase with respect to the wavelength and had a very large value (SSA > 0.9) during all the dusty days (two dust events, May 17, 2018; Fig. 20.5A and June 14, 2018; Fig. 20.5B) and had

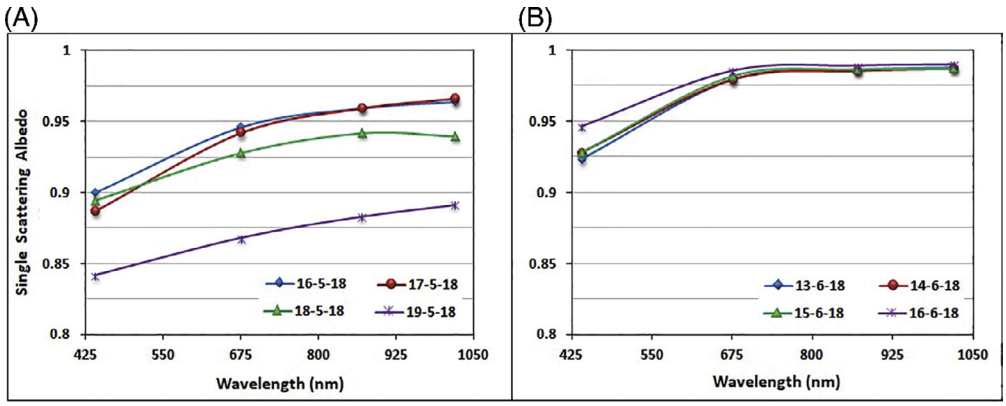

Fig. 20.5 Spectral variation of single scattering albedo (SSA) during the dust storm events (A) on May 18, 2018 and (B) on June 14, 2018 [43].

a very sharp increase at the time of the peak of dust events [2,42,43]. Larger the value of SSA greater than 0.90, alongside increasing fashion with wavelength, are traits of the dominance of dust aerosols particles inside the atmosphere [58].

At shorter wavelengths (440 nm), SSA reveals plenty of decreased values because of the large absorption of dust aerosol particles inside the UV and near-UV spectrum. A sharp upward increase of SSA value in the range of 440–675 nm wavelength clearly shows scattering nature of aerosol particles at a longer wavelength ($\lambda > 670$ nm) due to an increase in the concentration of coarse mode particles (high AOD, low AE) which is likewise shown from the daily variation of AOD (Fig. 20.3A), displaying higher AOD value (>1) at a higher wavelength which also confirms the dominance of coarse mode particles. Several studies have been reported by researchers which show a similar variation of SSA during the different dust events [16,42,43]. Kumar et al. [16] observed a comparable variety of SSA (≤0.95) throughout three specific dust activities in the pre-monsoon season (April 20, 28 May, and June 3, 2010) over Kanpur while over Karachi, Iftikhar et al. [59] observed much larger value of SSA approximately 0.98 throughout an extreme dust event (July 5, 2014).

20.3.2 Radiative characteristics

20.3.2.1 Aerosol radiative forcing (ARF) during major dust storms

Aerosol radiative forcing (ARF) is an essential atmospheric measure that indicates whether the atmosphere is warming or cooling. It is termed as the net difference in solar fluxes in the presence of aerosols and in the absence of aerosols whether it is at top of the atmosphere (TOA) or surface (BOA), respectively [60,61]. Recently, Kumar et al. [16] and Tiwari et al. [43] reported the change in the net radiation fluxes, during the different dust storm events and tried to calculate the ARF at the TOA and SRF with the help of the AERONET data over Kanpur using well-accepted widely used GAME (Global Atmospheric ModEl) radiative model [43] and SBDART model [16]. GAME is a widely used well-accepted radiative model that integrates the spectrum by using a correlated k-distribution based on line-by-line modeling [62], while the SBDART model is most widely used to calculate the change in the net radiation flux (only in the solar spectrum (0.25–4.0 μm) over Kanpur [63], based on very well profound physical models of radiation transmission and is widely used to calculate ARF. The SBDART model was running at 1-hour intervals over 24 hours, and daily ARF values at TOA and SRF were estimated in the days before and during the three dust storms periods (April 17–24, May 25–30, and May 31–June 4, 2010 [16]. The net difference between TOA and SRF force gives rise to the atmospheric forcing (heating or cooling) due to the absorption of light by the aerosol particles [43]. There are very important aerosol parameters that are necessary for calculating the ARF with the help of the SBDART model that involves the SSA, spectral AOD, and asymmetry factor, which could be obtained from the Kanpur AERONET station to achieve larger

accuracy within the ARF calculations. But, also there are some parameters utilized in the model that affects the radiative forcing are some of the astronomical factors (which involve sun elevation, azimuth, solar geometry, etc.) as well as the modeled atmosphere for the vertical distribution of temperature, pressure, surface albedo, and the humidity. Kumar et al. [16] found that the daily values for the total column ozone concentrations were calculated from the data extracted from the ozone monitoring instrument (OMI), onboard NASA's Aura satellite, and an average value was used for every dust event. The surface albedo value was obtained 0.15 from the Aura OMI version 3 reflectivity knowledge through the visualization from Giovanni's online data system. The general uncertainty within the calculable radiative forcing because of uncertainties in the input parameters was anticipated to be in the range of ~ 10%–15% [42]. Fig. 20.6 shows the daily variation of ARF during the major two dust-storm events in premonsoon in April 2010 (Fig. 20.6A) and in June 2018 (Fig. 20.6B). With the help of the above formulation, Kumar et al. [16] estimated the ARF values at SRF ranging from -31.85 to -101.60 W/m^2 (average -65.77 ± 21.72 W/m^2), at TOA -3.94 to -40.95 W/m^2 (average -17.99 ± 10.46 W/m^2), and within the atmosphere in the range of +16.87 to +75.11 W/m^2 (average +47.78 ± 16.24 W/m^2), respectively (Fig. 20.6A). But during April 20, May 28, and June 2, 2010, the ARF values were very high at TOA (-18.16, -40.95, and -29.58 W m^{-2}), at SRF (-93.27, -101.60, and -66.71 W/m^2), and within the atmosphere (+75.11, +60.65, and +37.13 W/m^2), whereas during the non-dusty days the ARF values were lower. Also, Tiwari et al. [43] estimated the ARF values at SRF (ranging from -101 to -191 W/m^2 (May 17, 2018) and -90 to -151 W/m^2 (June 14, 2018)), at TOA (-12 to -37 W/m^2 (May 17, 2018) and -47 to -64 W/m^2 (June 14, 2018)), and within the atmosphere in the range of (ARF_{ATM} = ~ +124 W/m^2 on May 17, 2018 and ARF_{ATM} = ~ +85 W/m^2 on June 14, 2018), respectively (Fig. 20.6B).

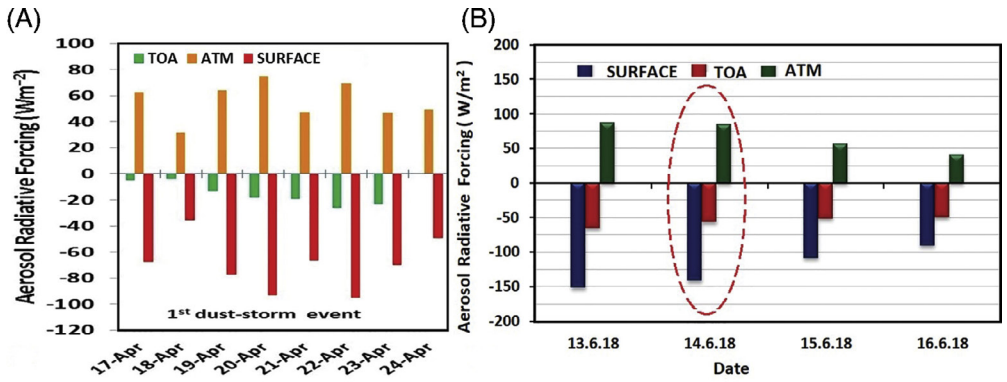

Fig. 20.6 Aerosol radiative forcing values (surface, top of the atmosphere and within the atmosphere in W/m^2) during the major two dust-storm events in premonsoon (A) ARF in April 2010 [16] and (B) ARF in June 2018 [43].

The above results show that because of the sudden increase in dust aerosol, the surface forcing increases (very large), whereas the part heating is very less affected, suggesting that the AOD plays the main role in ARF estimates throughout the dust events. Some of the previous studies are shown in Table 20.1 along with the aerosol characteristics and radiative forcing during different dust event and at different locations.

A significant modification in ARF is determined with the larger value of ARF (both at SRF and TOA) throughout each dusty day suggesting the additional attenuation of solar radiation (coming toward the surface), which can be due to the backscattering because of the dust aerosol particles. However, the positive value of ARF in the atmosphere suggests the net warming result of the atmosphere because of the dust aerosol during each event. Sharma et al. [33] found the ARF value as -100 W/m^2 to -50 W/m^2 at the surface and -25 W/m^2 to -10 W/m^2 at TOA over Patiala during the dust events of April 20–21, 2010 and May 26–28. The calculated ARF was higher than that of Kanpur, indicating an intense dust storm event over the western part of the IGB due to its proximity to dust source areas. Chinnam et al. [64] reported ARF values at SRF (-12 W/m^2) and TOA (+7 W/m^2) during the dusty days (May 12–22, 2004, Kanpur), showing the lower value at the SRF and showing the opposite signs for TOA compared to the above results. Furthermore, Prasad et al. [42] found ARF values in the range of -19 Wm^{-2} and -87 W/m^2 at SRF and +2 W/m^2 and -26 W/m^2 at TOA (during, April–May 2005).

Furthermore, the atmospheric heating rate was obtained by the following equation [16,43]:

$$\frac{\partial T}{\partial t} = \frac{g}{Cp}\frac{\Delta F_{Atmos}}{\Delta P} \tag{20.2}$$

where (in K/day) tells about the atmospheric heating rate, ΔF_{Atmos} describes the atmospheric forcing, g is the gravitational acceleration, Cp is the specific heat capacity of air (at constant pressure), and ΔP shows the pressure difference between top and bottom boundary of each layer of the atmosphere, whereas they had used ΔP as 300 hPa for the layer up to ~3.5 km that correspond to 1000–700 hPa pressure layer. With the help of Eq. (20.1), Kumar et al. [16] estimated the atmospheric heating rates with an average value of 1.33 K/day. The rates for atmospheric heating were reported very high during the dust storm events (April 20, May 28, and June 2, 2010) with the value 2.11 K/day, 1.70 K/day, and 1.04 K/day, respectively, while a very high value of the atmospheric heating rates (1.51–3.88 K/day and 0.9–1.88 K/day in May and June 2018, respectively) were reported by Tiwari et al. [43] showing very serious implications on climate. A similar range of the heating rate was also reported during the dust storm events over Delhi (1.9 K/day) and Jodhpur (2.0 K/day) [34] and over Lahore (1.3–2.2 K/day) and Karachi (0.7 to 1.4 K/day) [59]. Chinnam et al. [64] found anomalies in the rate of warming of the atmosphere in northern India during the premonsoon, mainly due to an increase in the number of dust particles, which contributed to affect the strengthening of the wind system (Indian monsoon). More detailed studies are needed on the effects of increased aerosol warming during the severe dust storm and its effects on regional climate.

20.4 Effect of dust storm

20.4.1 Effect of dust particle on health

Among all the particulate matter, finer one is very important which largely contributes to the adverse effect on human health. It has been noted that among most of the pollutants fine particles are repeatedly reported to be linked with adverse health impacts especially for mortality and morbidity for both globally [22–26,67,68] as well as in India [69–71]. The size of the dust particles is the key factor in determining the possible risk to human health [22]. Comparatively the course particles (size > 10 μm) are not breathable and affect our skin, eye conjunctivitis, and ophthalmic infection [22] whereas the fine particles (size < 10 μm) affect our internal organs causing Asthma, upper respiratory tract, cardiovascular disorder, etc [23,24]. There are very few researchers [68,72–74] have investigated the effect of multiple air pollutants and particulate matter like desert dust particles. Continuously, the concentration of fine particulate matter is increasing in the atmosphere from the natural as well as anthropogenic sources, which has decreased the air quality on regional to global scales [75]. It has been observed that the long-term variation of finer dust particles is associated with adverse health effects like heart disease and lung cancer which increases the risk of premature mortality [25,26]. The desert dust particles are one of the main natural sources of particulate matter which travel in the atmosphere in large amounts [76]. Through whole over the globe, in many regions, the concentration of $PM_{2.5}$ is much larger than the WHO [77] limit (10 $\mu g/m^3$) because of the regular dust events. In the World, the main dust sources (over 60% of the global dust load) are North Africa and the Middle East which causes a higher potential risk to the health of these regions because of their population [22]. South and East Asia have very high population density and these regions are also very often affected by severe dust events, but unfortunately in these regions, very few epidemiological studies have been done and adequate air quality data are lacking in the large amount [78]. Aerosol particles in terms of dust storms have detrimental impact on human health and agricultural activities in Central Asia [79]. It was reported that strong exposures to different particulate matters have major impact on human health [80,81]. However, under the National Air Quality Monitoring Programme, systematic monitoring of air quality indices such as $PM_{2.5}$, PM_{10}, NO_2, SO_2, and O_3 is now available in most Indian cities [82]. Therefore it is much needed to study the effect of atmospheric pollutants especially particulate matter on health.

20.4.2 Effect of a dust particle on climate

Dust particles scatter as well as absorb the solar radiation coming from the Sun. Scattering dust particles cause a cooling effect whereas absorbing dust particles show a warming effect. Dust particles play a vital role in the formation of clouds as they provide cloud condensation nuclei (CCN). A large number of dust particles may increase the number concentration of CCN through which cloud droplet is formed [83]. The cooling and warming effect occurs due to cloud droplets and their characteristics. So dust particles

affect the planet's radiation balance and thus changing in climate occur [84]. A dust storm is a natural process but sand dust aerosols produced by man-made sources also affect the climate. Sand dust particles affect the radiation of the local atmosphere as well as the monsoon system, local water cycle, and regional climate environment [85]. Agriculture and the ecosystem are also affected by the dust storm. The size of the dust particle is equivalent to the wavelength of visible light which shows the scattering nature that minimizes the visibility of the atmosphere at the regional level [86]. Apart from its negative health impacts, coarse mode particle is responsible for lowering atmospheric clarity as a key element of smog, diminishing the photosynthesis process through accumulation on the surface of leaves, and trying to influence atmospheric chemistry and climatological processes [87–89]. The resulting decrease in air quality has an influence on social and economic sectors as well as marine and air transportation [90].

20.5 Summary and conclusion

The outcomes introduced in this section show effect of dust on the condition of the climate, environment, and human health. Because of dust storms, diverse atmospheric parameters (precipitation, wind speed, wind direction, humidity, atmospheric temperature, and so forth) are profoundly influenced which debases the air quality. The dust is moved from the source to an excessively far away distance influencing individuals living along the track of dust and the state of the weather conditions. The air quality influences extraordinarily the strength of human health, which is viewed as a drawn-out long-term health hazard. Remote sensing satellites with multisensors cover the globe in a couple of hours, and the satellite information gives data about the various parameters (AOD, AE, AVSD, ARF, and so on) by which condition of the weather can be found and this information can be utilized for observing dust transport from the source to distant locals influenced by dust. This information can be utilized for observing dust storms and offering warnings to individuals about dust and the power of dust storms so that individuals would not be uncovered and experience the ill effects of bad air quality. With the worldwide climate change, land use and land cover are changing which is probably going to build recurrence of dust storms and their force.

Acknowledgment

The work is financially supported by the Institute of Eminence (IoE) (Scheme No: 6031) to BHU,Varanasi.

References

[1] P. Ginoux, J.M. Prospero, T.E. Gill, N.C. Hsu, M. Zhao, Global-scale attribution of anthropogenic and natural dust sources and their emission rates based on MODIS Deep Blue aerosol products, Rev. Geophys. *50* (RG3005) (2012) 1–36.

[2] S. Dey, S.N. Tripathi, R.P. Singh, B.N. Holben, Influence of dust storms on the aerosol optical properties over the Indo-Gangetic basin, Journal of Geophysical Research: Atmospheres *109* (D20211) (2004) 1–13.

[3] R.P. Singh, S. Dey, S.N. Tripathi, V. Tare, B. Holben, Variability of aerosol parameters over Kanpur, northern India, Journal of Geophysical Research: Atmospheres *109* (D23206) (2004) 1–14.
[4] N. Huneeus, M. Schulz, Y. Balkanski, J. Griesfeller, J. Prospero, S. Kinne, S. Bauer, O. Boucher, M. Chin, F. Dentener, T. Diehl, R. Easter, D. Fillmore, S. Ghan, P. Ginoux, A. Grini, L. Horowitz, D. Koch, M.C. Krol, W. Landing, X. Liu, N. Mahowald, R. Miller, J.J. Morcrette, G. Myhre, J. Penner, J. Perlwitz, P. Stier, T. Takemura, C.S. Zender, Global dust model intercomparison in AeroCom phase I, Atmos. Chem. Phys. *11* (15) (2011) 7781–7816.
[5] W. Wang, L. Sheng, H. Jin, Y. Han, Dust aerosol effects on cirrus and altocumulus clouds in Northwest China, Journal of Meteorological Research *29* (5) (2015) 793–805.
[6] S. Tiwari, A.K. Mishra, A.K. Singh, Aerosol climatology over the Bay of Bengal and Arabian Sea inferred from space-borne radiometers and lidar observations, Aerosol and Air Quality Research *16* (11) (2016) 2855–2868.
[7] V. Ramanathan, C. Chung, D. Kim, T. Bettge, L. Buja, J.T. Kiehl, W.M. Washington, Q. Fu, D.R. Sikka, M. Wild, Atmospheric brown clouds: Impacts on South Asian climate and hydrological cycle, Proc. Natl. Acad. Sci. *102* (15) (2005) 5326–5333.
[8] M. Carugno, D. Consonni, G. Randi, D. Catelan, L. Grisotto, P.A. Bertazzi, A. Biggeri, M. Baccini, Air pollution exposure, cause-specific deaths and hospitalizations in a highly polluted Italian region, Environ. Res. *147* (2016) 415–424.
[9] A.S. Goudie, N.J. Middleton, Desert Dust in the Global System, 1st ed., Springer Science & Business Media, Heidelberg, 2006.
[10] Y. Shao, K.H. Wyrwoll, A. Chappell, J. Huang, Z. Lin, G.H. McTainsh, M. Mikami, T.Y. Tanaka, X. Wangh, S. Yoon, Dust cycle: an emerging core theme in Earth system science, Aeolian Res. *2* (4) (2011) 181–204.
[11] T.H. Painter, S.M. Skiles, J.S. Deems, W.T. Brandt, J. Dozier, Variation in rising limb of Colorado River snowmelt runoff hydrograph controlled by dust radiative forcing in snow, Geophys. Res. Lett. *45* (2) (2018) 797–808.
[12] N. Middleton, Dust storm hazards, E3S Web of Conferences, 99, EDP Sciences, 2019, pp. 04001.
[13] N.J. Middleton, A geography of dust storms in South-west Asia, Journal of Climatology *6* (2) (1986) 183–196.
[14] S.K. Mishra, S.N. Tripathi, Modeling optical properties of mineral dust over the Indian Desert, Journal of Geophysical Research: Atmospheres *113* (D23) (2008).
[15] S.C. Tan, J. Li, H. Che, B. Chen, H. Wang, Transport of East Asian dust storms to the marginal seas of China and the southern North Pacific in spring 2010, Atmos. Environ. *148* (2017) 316–328.
[16] S. Kumar, S. Kumar, D.G. Kaskaoutis, R.P. Singh, R.K. Singh, A.K. Mishra, M.K. Srivastava, A.K. Singh, Meteorological, atmospheric and climatic perturbations during major dust storms over Indo-Gangetic Basin, Aeolian Res. *17* (2015) 15–31.
[17] K. Taneja, S. Ahmad, K. Ahmad, S.D. Attri, Impact assessment of a severe dust storm on atmospheric aerosols over an urban site in India, Curr. Sci. *118* (5) (2020) 737.
[18] M.A. Aswini, A. Kumar, S.K. Das, Quantification of long-range transported aeolian dust towards the Indian peninsular region using satellite and ground-based data-A case study during a dust storm over the Arabian Sea, Atmos. Res. *239* (2020) 104910.
[19] K. Suresh, U. Singh, A. Kumar, D. Karri, A. Peketi, V. Ramaswamy, Provenance tracing of long-range transported dust over the Northeastern Arabian Sea during the southwest monsoon, Atmos. Res. *250* (2021) 105377.
[20] A. Kumar, K. Suresh, W. Rahaman, Geochemical characterization of modern aeolian dust over the Northeastern Arabian Sea: implication for dust transport in the Arabian Sea, Sci. Total Environ. *729* (2020) 138576.
[21] P.S. Bhattacharjee, A.K. Prasad, M. Kafatos, R.P. Singh, Influence of a dust storm on carbon monoxide and water vapor over the Indo-Gangetic Plains, Journal of Geophysical Research: Atmospheres *112* (D18203) (2007) 1–14.
[22] D. Giannadaki, A. Pozzer, J. Lelieveld, Modeled global effects of airborne desert dust on air quality and premature mortality, Atmos. Chem. Phys. *14* (2) (2014) 957–968.
[23] C.A. Pope III, M. Ezzati, D.W Dockery, Fine-particulate air pollution and life expectancy in the United States, N. Engl. J. Med. *360* (4) (2009) 376–386.

[24] J. Lepeule, F. Laden, D. Dockery, J. Schwartz, Chronic exposure to fine particles and mortality: an extended follow-up of the Harvard Six Cities study from 1974 to 2009, Environ. Health Perspect. *120* (7) (2012) 965–970.
[25] A.J. Cohen, H.R. Anderson, B. Ostra, K.D. Pandey, M. Krzyzanowski, N. Künzli, K. Gutschmidt, A. Pope, I. Romieu, J.M. Samet, K. Smith, The global burden of disease due to outdoor air pollution, J. Toxicol. Environ. Health Part A *68* (13-14) (2005) 1301–1307.
[26] D. Krewski, M. Jerrett, R.T. Burnett, R. Ma, E. Hughes, Y. Shi, M.C. Turner, C.A. Pope III, G. Thurston, E.E. Calle, M.J Thun, Extended follow-up and spatial analysis of the American Cancer Society study linking particulate air pollution and mortality, 140, Health Effects Institute, Boston, MA, 2009.
[27] S. Namdari, N. Karimi, A. Sorooshian, G. Mohammadi, S. Sehatkashani, Impacts of climate and synoptic fluctuations on dust storm activity over the Middle East, Atmos. Environ. *173* (2018) 265–276.
[28] A. Singh, S. Tiwari, D. Sharma, D. Singh, S. Tiwari, A.K. Srivastava, N. Rastogi, A.K. Singh, Characterization and radiative impact of dust aerosols over northwestern part of India: a case study during a severe dust storm, Meteorol. Atmos. Phys. *128* (6) (2016) 779–792.
[29] S. Tiwari, A.K. Srivastava, A.K. Singh, S. Singh, Identification of aerosol types over Indo-Gangetic Basin: implications to optical properties and associated radiative forcing, Environmental Science and Pollution Research *22* (16) (2015) 12246–12260.
[30] A.K. Prasad, R.P. Singh, Changes in aerosol parameters during major dust storm events (2001–2005) over the Indo-Gangetic Plains using AERONET and MODIS data, Journal of Geophysical Research: Atmospheres *112* (D09208) (2007) 1–18.
[31] A.K. Srivastava, P. Pant, P. Hegde, S. Singh, U.C. Dumka, M. Naja, N. Singh, Y. Bhavanikumar, The influence of a south Asian dust storm on aerosol radiative forcing at a high-altitude station in central Himalayas, Int. J. Remote Sens. *32* (22) (2011) 7827–7845.
[32] G.R. Aher, G.V. Pawar, P. Gupta, P.C.S. Devara, Effect of major dust storm on optical, physical, and radiative properties of aerosols over coastal and urban environments in Western India, Int. J. Remote Sens. *35* (3) (2014) 871–903.
[33] D. Sharma, D. Singh, D.G. Kaskaoutis, Impact of two intense dust storms on aerosol characteristics and radiative forcing over Patiala, northwestern India, Adv. Meteorol., *2012*, Hindawi, 2012, pp. 1–13 956814.
[34] A.K. Srivastava, V.K. Soni, S. Singh, V.P. Kanawade, N. Singh, S. Tiwari, S.D. Attri, An early South Asian dust storm during March 2012 and its impacts on Indian Himalayan foothills: A case study, Sci. Total Environ. *493* (2014) 526–534.
[35] J.M. Prospero, P. Ginoux, O. Torres, S.E. Nicholson, T.E. Gill, Environmental characterization of global sources of atmospheric soil dust identified with the Nimbus 7 Total Ozone Mapping Spectrometer (TOMS) absorbing aerosol product, Rev. Geophys. *40* (1) (2002) 2 -1.
[36] B.N. Holben, T.F. Eck, I. Slutsker, D. Tanré, J.P. Buis, A. Setzer, E. Vermote, J.A. Reagan, Y.J. Kaufman, T. Nakajima, F. Lavenu, I. Jankowiak, A. Smirnov, AERONET—A federated instrument network and data archive for aerosol characterization, Remote Sens. Environ. *66* (1) (1998) 1–16.
[37] O. Dubovik, M.D. King, A flexible inversion algorithm for retrieval of aerosol optical properties from Sun and sky radiance measurements, Journal of Geophysical Research: Atmospheres *105* (D16) (2000) 20673–20696.
[38] A. Smirnov, B.N. Holben, T.F. Eck, O. Dubovik, I. Slutsker, Cloud-screening and quality control algorithms for the AERONET database, Remote Sens. Environ. *73* (3) (2000) 337–349.
[39] O. Dubovik, A. Smirnov, B.N. Holben, M.D. King, Y.J. Kaufman, T.F. Eck, I. Slutsker, Accuracy assessments of aerosol optical properties retrieved from Aerosol Robotic Network (AERONET) Sun and sky radiance measurements, Journal of Geophysical Research: Atmospheres *105* (D8) (2000) 9791–9806.
[40] T.F. Eck, B.N. Holben, J.S. Reid, O. Dubovik, A. Smirnov, N.T. O'Neill, I. Slutsker, S. Kinne, Wavelength dependence of the optical depth of biomass burning, urban, and desert dust aerosols, Journal of Geophysical Research: Atmospheres *104* (D24) (1999) 31333–31349.
[41] K. Alam, T. Trautmann, T. Blaschke, F. Subhan, Changes in aerosol optical properties due to dust storms in the Middle East and Southwest Asia, Remote Sens. Environ. *143* (2014) 216–227.
[42] A.K. Prasad, S. Singh, S.S. Chauhan, M.K. Srivastava, R.P. Singh, R. Singh, Aerosol radiative forcing over the Indo-Gangetic plains during major dust storms, Atmos. Environ. 41 (2007) 6289–6301.
[43] S. Tiwari, A. Kumar, V. Pratap, A.K. Singh, Assessment of two intense dust storm characteristics over Indo–Gangetic basin and their radiative impacts: a case study, Atmos. Res. *228* (2019) 23–40.

[44] R.P. Singh, Dust storms and their influence on atmospheric parameters over the Indo-Gangetic plains. In: Geospatial technologies and climate change, Springer, Cham, 2014, pp. 21–35.
[45] S. Bucci, C. Cagnazzo, F. Cairo, L. Di Liberto, F. Fierli, Aerosol variability and atmospheric transport in the Himalayan region from CALIOP 2007–2010 observations, Atmos. Chem. Phys. *14* (9) (2014) 4369–4381.
[46] D. Liu, Y. Wang, Z. Wang, J. Zhou, The three-dimensional structure of transatlantic African dust transport: A new perspective from CALIPSO LIDAR measurements, Advances in Meteorology *2012* (2012).
[47] D.M. Winker, W.H. Hunt, M.J. McGill, Initial performance assessment of CALIOP, Geophys. Res. Lett. *34* (19) (2007).
[48] A.H. Omar, D.M. Winker, M.A. Vaughan, Y. Hu, C.R. Trepte, R.A. Ferrare, Z. Liu, The CALIPSO automated aerosol classification and lidar ratio selection algorithm, J. Atmos. Oceanic Technol. *26* (10) (2009) 1994–2014.
[49] A.K. Mishra, T. Shibata, Climatological aspects of seasonal variation of aerosol vertical distribution over central Indo-Gangetic belt (IGB) inferred by the space-borne lidar CALIOP, Atmos. Environ. *46* (2012) 365–375.
[50] R.R. Draxler, G.D. Hess, An overview of the HYSPLIT_4 modelling system for trajectories, Australian meteorological magazine *47* (4) (1998) 295–308.
[51] A.F. Stein, R.R. Draxler, G.D. Rolph, B.J. Stunder, M.D. Cohen, F. Ngan, NOAA's HYSPLIT atmospheric transport and dispersion modeling system, Bull. Am. Meteorol. Soc. *96* (12) (2015) 2059–2077.
[52] Draxler, R. R., & Rolph, G. D. (2003). HYSPLIT (HYbrid Single-Particle Lagrangian Integrated Trajectory) model access via NOAA ARL READY (https://www.arl.noaa.gov/ready/hysplit4.html). NOAA Air Resources Laboratory, Silver Spring.
[53] A. Ångström, The parameters of atmospheric turbidity, Tellus *16* (1) (1964) 64–75.
[54] S. Tiwari, D. Kaskaoutis, V.K. Soni, S. Dev Attri, A.K. Singh, Aerosol columnar characteristics and their heterogeneous nature over Varanasi, in the central Ganges valley, Environmental Science and Pollution Research *25* (25) (2018) 24726–24745.
[55] K. Alam, T. Trautmann, T. Blaschke, H. Majid, Aerosol optical and radiative properties during summer and winter seasons over Lahore and Karachi, Atmos. Environ. *50* (2012) 234–245.
[56] T. Takemura, T. Nakajima, O. Dubovik, B.N. Holben, S. Kinne, Single-scattering albedo and radiative forcing of various aerosol species with a global three-dimensional model, Journal of Climate *15* (4) (2002) 333–352.
[57] O. Dubovik, B.N. Holben, Y.J. Kaufman, M. Yamasoe, A. Smirnov, D. Tanré, I. Slutsker, Single-scattering albedo of smoke retrieved from the sky radiance and solar transmittance measured from ground, Journal of Geophysical Research: Atmospheres *103* (D24) (1998) 31903–31923.
[58] O. Dubovik, B.N. Holben, T.F. Eck, A. Smirnov, Y.J. Kaufman, M.D. King, D. Tanre, I. Slutsker, Variability of absorption and optical properties of key aerosol types observed in worldwide locations, J. Atmospheric Sci. *59* (3) (2002) 590–608.
[59] M. Iftikhar, K. Alam, A. Sorooshian, W.A. Syed, S. Bibi, H. Bibi, Contrasting aerosol optical and radiative properties between dust and urban haze episodes in megacities of Pakistan, Atmos. Environ. *173* (2018) 157–172.
[60] K. Alam, T. Trautmann, T. Blaschke, H. Majid, Aerosol optical and radiative properties during summer and winter seasons over Lahore and Karachi, Atmos. Environ. *50* (2012) 234–245.
[61] A. Kumar, V. Pratap, S. Kumar, A.K. Singh, Atmospheric aerosols properties over Indo-Gangetic Plain: a trend analysis using ground–truth AERONET data for the year 2009-2017, Adv. Space Res. *69* (7) (2022) 2659–2670.
[62] N.A. Scott, A direct method of computation of the transmission function of an inhomogeneous gaseous medium—I: Description of the method, J. Quant. Spectrosc. Radiat. Transfer *14* (8) (1974) 691–704.
[63] P. Ricchiazzi, S. Yang, C. Gautier, D. Sowle, SBDART: A research and teaching software tool for plane-parallel radiative transfer in the Earth's atmosphere, Bull. Am. Meteorol. Soc. *79* (10) (1998) 2101–2114.
[64] N. Chinnam, S. Dey, S.N. Tripathi, M. Sharma, Dust events in Kanpur, northern India: chemical evidence for source and implications to radiative forcing, Geophys. Res. Lett. *33* (L08803) (2006) 1–4.

[65] S.K. Srivastava, M.K. Srivastava, A. Saha, S. Tiwari, S. Singh, U.C. Dumka, B.P. Singh, N.P Singh, Aerosol optical properties over Delhi and Manora Peak during a rare dust event in early April 2005, Int. J. Remote Sens. *32* (23) (2011) 7939–7954.
[66] S. Singh, S. Naseema Beegum, Direct radiative effects of an unseasonal dust storm at a western Indo Gangetic Plain station Delhi in ultraviolet, shortwave, and longwave regions, Geophys. Res. Lett. *40* (10) (2013) 2444–2449.
[67] K.R. Smith, M. Jerrett, H.R. Anderson, R.T. Burnett, V. Stone, R. Derwent, W.A. Richard, C. Aaron, B.S.MPH Seth, K. Daniel, P. Arden, J.T.M.D. Micael, G. Thurston, Public health benefits of strategies to reduce greenhouse-gas emissions: health implications of short-lived greenhouse pollutants, Lancet North Am. Ed. *374* (9707) (2009) 2091–2103.
[68] N.A.H. Janssen, G. Hoek, M. Simic-Lawson, P. Fischer, L.Van Bree, B. Harry ten, M. Keuken, R.W. Atkinson, H.R. Anderson, B. Brunekreef, F.R. Cassee, Black carbon as an additional indicator of the adverse health effects of airborne particles compared with PM10 and PM2. 5, Environ. Health Perspect. *119* (12) (2011) 1691–1699.
[69] S. Chowdhury, S. Dey, K.R. Smith, Ambient PM2. 5 exposure and expected premature mortality to 2100 in India under climate change scenarios, Nat. Commun. *9* (1) (2018) 1–10.
[70] K. Balakrishnan, S. Dey, T. Gupta, R.S. Dhaliwal, M. Brauer, A.J. Cohen, J.D. Stanaway, G. Beig, T.K. Joshi, A.N. Aggarwal, Y. Sabde, The impact of air pollution on deaths, disease burden, and life expectancy across the states of India: the Global Burden of Disease Study 2017, The Lancet Planetary Health *3* (1) (2019) e26–e39.
[71] P. Saini, M. Sharma, Cause and Age-specific premature mortality attributable to PM2.5 Exposure: an analysis for Million-Plus Indian cities, Sci. Total Environ. *710* (2020) 135230.
[72] J. Cao, H. Xu, Q. Xu, B. Chen, H. Kan, Fine particulate matter constituents and cardiopulmonary mortality in a heavily polluted Chinese city, Environ. Health Perspect. *120* (3) (2012) 373–378.
[73] X. Wang, R. Chen, X. Meng, F. Geng, C. Wang, H. Kan, Associations between fine particle, coarse particle, black carbon and hospital visits in a Chinese city, Sci. Total Environ. *458* (2013) 1–6.
[74] J. Lelieveld, J.S. Evans, M. Fnais, D. Giannadaki, A. Pozzer, The contribution of outdoor air pollution sources to premature mortality on a global scale, Nature *525* (7569) (2015) 367–371.
[75] H. Akimoto, Global air quality and pollution, Science *302* (5651) (2003) 1716–1719.
[76] N.M. Mahowald, S. Kloster, S. Engelstaedter, J.K. Moore, S. Mukhopadhyay, J.R. McConnell, S. Albani, S.C. Doney, A. Bhattacharya, M.A.J. Curran, M.G. Flanner, F.M. Hoffman, D.M. Lawrence, K. Lindsay, P.A. Mayewski, J. Neff, D. Rothenberg, E. Thomas, P.E. Thornton, C.S. Zender, Observed 20th century desert dust variability: impact on climate and biogeochemistry, Atmos. Chem. Phys. *10* (22) (2010) 10875–10893.
[77] WHO, Air Quality Guidelines, World Health Organization, 2005, http://www.euro.who.int/__data/assets/pdf_file/0005/78638/E90038.pdf Global update.
[78] F. De Longueville, Y.C. Hountondji, S. Henry, P. Ozer, What do we know about effects of desert dust on air quality and human health in West Africa compared to other regions? Sci. Total Environ. *409* (1) (2010) 1–8.
[79] B. Sobhani, V.S. Zengir, Investigation hazard effect of monthly ferrrin temperature on agricultural products in north bar of Iran, The Iraqi Journal of Agricultural Science *50* (1) (2019) 320–330.
[80] K. Balakrishnan, S. Dey, T. Gupta, R.S. Dhaliwal, M. Brauer, A.J. Cohen, J.D. Stanaway, G. Beig, T.K. Joshi, A.N. Aggarwal, Y. Sabde, The impact of air pollution on deaths, disease burden, and life expectancy across the states of India: the Global Burden of Disease Study 2017, The Lancet Planetary Health *3* (1) (2019) e26–e39.
[81] J. Huang, X. Pan, X. Guo, G. Li, Impacts of air pollution wave on years of life lost: a crucial way to communicate the health risks of air pollution to the public, Environ. Int. *113* (2018) 42–49.
[82] N. Singh, A. Mhawish, T. Banerjee, S. Ghosh, R.S. Singh, R.K. Mall, Association of aerosols, trace gases and black carbon with mortality in an urban pollution hotspot over central Indo-Gangetic Plain, Atmos. Environ. *246* (2021) 118088.
[83] S. Twomey, The influence of pollution on the shortwave Albedo of Clouds, Journal of Atmospheric Sciences *34* (7) (1977) 1149–1152.
[84] M.O. Andreae, P.J. Crutzen, Atmospheric aerosols: Biogeochemical sources and role in atmospheric chemistry, Science *276* (5315) (1997) 1052–1058.

[85] K. Zhang, H. Gao, R. Zhang, Y. ZHU, Y. WANG, Sources and movement routes of sand-dust aerosols and their impact probabilities on China seas in 2000-2002, Advances in Earth Science *20* (6) (2005) 627.
[86] O. Uchino, I. Tabata, Mobile lidar for simultaneous measurements of ozone, aerosols, and temperature in the stratosphere, Appl. Opt. *30* (15) (1991) 2005–2012.
[87] D.A. Grantz, J.H.B. Garner, D.W. Johnson, Ecological effects of particulate matter, Environ. Int. *29* (2-3) (2003) 213–239.
[88] M. Lin, J. Tao, C.Y. Chan, J.J. Cao, Z.S. Zhang, L.H. Zhu, R.J. Zhang, Regression analyses between recent air quality and visibility changes in megacities at four haze regions in China, Aerosol and air quality research *12* (6) (2012) 1049–1061.
[89] E. Von Schneidemesser, P.S. Monks, J.D. Allan, L. Bruhwiler, P. Forster, D. Fowler, A. Lauer, W.T. Morgan, P. Paasonen, M. Righi, K. Sindelarova, M.A. Sutton, Chemistry and the linkages between air quality and climate change, Chem. Rev. *115* (10) (2015) 3856–3897.
[90] F. Zhang, Q.R. Yu, J.L. Mao, C. Dan, Y. Wang, Q. He, T. Cheng, C. Chen, D. Liu, Y. Gao, Possible mechanisms of summer cirrus clouds over the Tibetan Plateau, Atmos. Chem. Phys. *20* (20) (2020) 11799–11808.